Two-photon polymerization nanofabrication of ultracompact light scattering spectroscopic probe for detection of pre-cancer in pancreatic cyst

Conor J. Sheil^{1†}, Umar Khan^{1†}, Yuri N. Zakharov¹, Mark F. Coughlan¹, Douglas K. Pleskow², Mandeep S. Sawhney², Tyler M. Berzin², Jonah M. Cohen², Maria Glyavina¹, Lei Zhang¹, Irving Itzkan¹, Lev T. Perelman^{1,2}, and Le Qiu^{1*}

¹Center for Advanced Biomedical Imaging and Photonics Division of Gastroenterology, Department of Medicine Beth Israel Deaconess Medical Center Harvard University

²Center for Advanced Endoscopy
Division of Gastroenterology, Department of Medicine
Beth Israel Deaconess Medical Center
Harvard University

³Biological and Biomedical Sciences Program Harvard University

*Corresponding author: Le Qiu

Assistant Professor and Assistant Director

Center for Advanced Biomedical Imaging and Photonics Division of Gastroenterology, Department of Medicine

Beth Israel Deaconess Medical Center

Harvard University

lqiu@bidmc.harvard.edu phone: 617.667.8227

[†]These authors contributed equally to this work

Abstract:

Pancreatic cancer has one of the worst survival rates of all major cancers, with pancreatic

cystic lesions accounting for one in three pancreatic surgeries. The current gold-standard

for diagnosis of pancreatic cyst malignancy is based on the endoscopic ultrasound guided

fine-needle aspiration (EUS-FNA) procedure, which suffers from a low accuracy in detecting

malignancy. Here we present the design and two-photon polymerization based fabrication

of refractive and reflective non-contact probes, capable of rapid surveillance of the entire

internal cyst surface-an advance over the contact probe we recently developed that allowed,

for the first time, reliable evaluation of pancreatic cyst malignant potential in vivo. We

employed a novel two-photon polymerization technique, which allows direct laser-writing to

an accuracy of tens of nanometers, to fit the probe within the 540 micrometer internal

diameter EUS-FNA needle. The newly constructed probes show excellent separation of the

illumination and collection beams, essential for proper operation of the spatial gating

method. These probes can be used clinically to perform rapid "optical biopsy", ultimately

eliminating unnecessary pancreatic surgeries on benign cysts and dangerous delays in

surgical removal of malignant cysts, improving patient prognosis and quality of life.

Keywords: light scattering, two-photon polymerization, nanofabrication, probe, cancer

2

1. INTRODUCTION

The global incidence of pancreatic cancer is rising yearly—by 2030, the death rate of pancreatic cancer is predicted to be second highest of all cancer deaths in the United States [1]. While the treatment of several common cancers has drastically improved in recent years, pancreatic cancer has one of the worst survival rates of all major cancers [2] due to lack of early diagnosis and treatment. Pancreatic cystic lesions are found in greater than 2% of the adult population [3] and account for one in three pancreatic surgeries [4]. Such lesions are often found at a treatable early stage by non-invasive methods such as magnetic resonance imaging (MRI) and computed tomography (CT); however, these techniques are limited in their ability to identify the type of pancreatic cyst. As a result, distinguishing between benign, cancerous and precancerous cysts with sufficient accuracy in a reasonable time period is currently not possible with any diagnostic technique. This inherent uncertainty results in a substantial number of non-essential pancreatic surgeries involving benign cysts, and dangerous delays in surgical removal of malignant cysts. The current gold-standard for diagnosis of pancreatic cyst malignancy is based on endoscopic ultrasound guided fineneedle aspiration (EUS-FNA). Performed in nine out of ten cases that require a decision on surgery, the EUS-FNA procedure suffers from a low accuracy in detecting malignancy, of less than 50% [4,5]. The low accuracy of EUS-FNA cytopathology highlights the crucial need for a more accurate diagnostic tool compatible with the EUS-FNA procedure.

The spatial gating light scattering spectroscopic (LSS) fiber optic probe we recently developed and tested in human subjects provides such a tool [6]. It detects spectra of light elastically scattered by epithelial tissue, which consist of two principal components: a diffuse scattering component originating in the submucosal tissue, and a backscattering component originating in the epithelial cells, the latter of which contains useful information about

morphology of the cellular nucleus and the rest of the organelles. This backscattering signal, which has been shown to be useful for early malignancy diagnosis [6], can be isolated from the large diffuse background using various gating techniques [7–13].

One of the problems associated with early detection of cancer using fiber optics probes, in combination with various endoscopic devices, is the difficulty in accessing certain organs such as the pancreas. This generates a conflicting requirement to deliver probes that use the sub-millimeter size working channels of clinical instruments, and that can also detect light scattering spectroscopic signals from large areas of tissue in the short time permitted for the procedure. For example, the existing spatial gating LSS fiber optic probe [6] identifies the malignant potential of pancreatic cysts by entering through the needle used during the routine diagnostic minimally invasive EUS-FNA procedure. It employs a single-point forward-looking spatial gating contact probe that fits into a standard 22-gauge aspiration needle and samples a fraction of the internal surface of the cyst forward-hemisphere, measuring 10 to 20 locations in approximately 2 minutes. To improve accuracy of the optical biopsy, scanning the entire internal cyst surface in a shorter time with a side-looking non-contact spatial gating LSS fiber optic probe (Fig. 1) would be a significant advance.

We envision that the clinical measurements with side-looking probes will be performed in patients undergoing pancreatic cyst EUS-FNA procedures. The procedure could be performed as in the following brief description. Prior to the procedure, the probe will be inserted into the 22-gauge FNA needle and secured with a fixed-length tube to ensure that its distal end is stowed safely inside the FNA needle. The probe proximal end will then be connected to the instrument control system. The endoscope will be introduced to the duodenum; and, after a pancreatic EUS examination, the FNA needle will be inserted and

used for a transduodenal puncture of the cyst. The endoscopist will position the needle at the cyst entrance wall and extend the probe toward the opposite wall, using a foot pedal to operate the instrument.

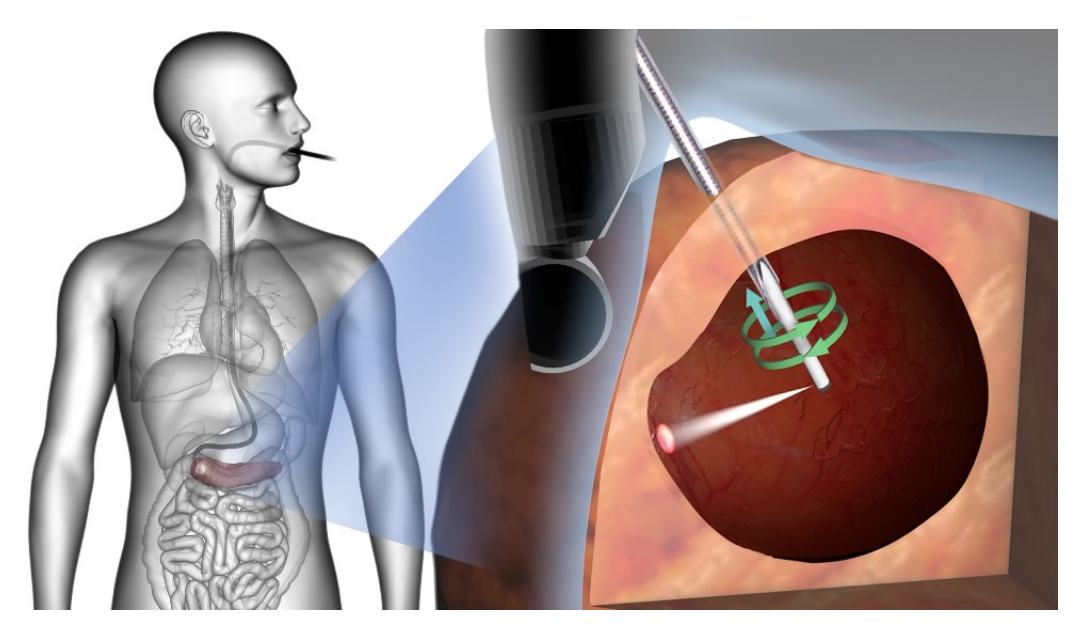


Fig. 1. Illustration of the proposed side-looking non-contact LSS fiber optic probe scanning the entire cyst internal surface. Left side shows the position of the endoscope and insertion of the FNA needle with probe. Inset shows an expanded view of the probe scan (clockwise and counterclockwise rotations and linear translation).

The number of probe translational scan steps and the variable step size of the linear scan will be determined in the instrument software, based on the cyst size, to ensure 30% overlap of adjacent spots and an even coverage of the entire cyst internal surface. Each 360° clockwise rotation of the probe will be followed by a linear retraction step and a 360° counterclockwise rotation (see Fig. 1 inset). The scanning in the counterclockwise direction will be possible due to the linear response of the torque tube. The side-looking scanning probe will perform optical biopsy on approximately 300 sites in a 3 cm diameter cyst, interrogating its entire internal surface in approximately 30 seconds. Though knowledge about the precise location of cells with a malignant potential within a cyst is not needed,

the capability of the proposed probe to perform point-by-point scanning of the surface of the cyst will be important for detecting focal disease. Also, spatial gating enhances the contribution of the upper, several hundred micron thick, epithelial tissue layer where early-stage epithelial lesions such as cystic precursor lesions in the pancreas are confined. After the scanning, the probe will be removed from the FNA needle and the cyst fluid collected in the standard fashion to be sent for cytological and biochemical analysis.

The goal of the current work was to design and fabricate a side-looking non-contact LSS probe to fit comfortably within a rather small 22-gauge needle (540 µm internal diameter), with the significant challenge of designing and incorporating ultra-small optics to fold and collimate the light beams for collection and delivery. Fabrication of such a device is not possible with conventional means due to the prohibitively large sizes of typical results. This task is hence ideally suited to the relatively new technology of two-photon polymerization nanofabrication [14]. The two-photon polymerization nanofabrication system is essentially a two-photon microscope where, instead of the focal volume scanning across a sample of interest, it is scanned within a drop of resin, which is cured by the two-photon interaction. It allows nanofabrication of optical-grade components as large as 8 mm in length with a spatial resolution as fine as 40 nm [14]. Crucially, this type of nanofabrication allows fabrication of both optical and non-optical components simultaneously in a single package, removing the step of aligning the micro-components, which is exceedingly difficult at such small scales.

2. MATERIALS AND METHODS

2.1 Basic principles of the optical design of spatial gating non-contact probes

The single-point forward-looking contact spatial gating LSS probe we recently developed and tested in human subjects [6] consists of a bundle of seven optical fibers: one central fiber surrounded by a hexagonally arranged ring, each with a core diameter of $100~\mu m$ and a numerical aperture (NA) of 0.21. A fiber in the outer hexagon delivers light to the pancreas lining, while three of the remaining fibers are used to collect light, forming source-detector distances of 120, 220 and $240~\mu m$, respectively, to achieve spatial gating. Because the ends of the fibers are polished flat, the delivered light is not focused or collimated; therefore, for correct operation, the probe needs to be positioned in close proximity to the pancreas inner lining, limiting the area it can access at a time—to collect multiple "optical biopsies", the probe must be moved to new locations on the cyst wall.

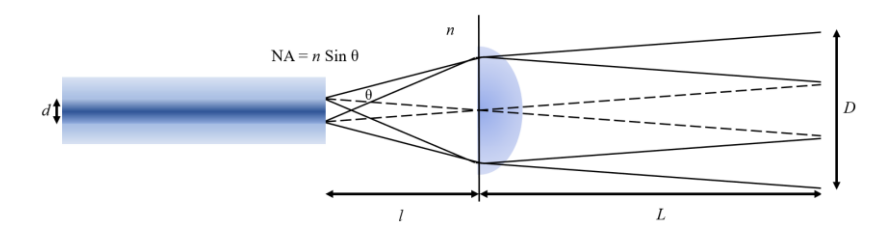


Fig. 2. Schematic diagram of the contributions of fiber NA and diameter d to tissue illumination spot diameter D. The tissue is a distance L from the collimating lens, which is a distance I from the fiber.

Fundamental to the operation of the spatial gating probe is proper separation of the source and detection light beams, which is comparable to the distance light travels in tissue between scattering events. In the case of the contact probe, this is simply a case of separating the source and collection fibers; however, the non-contact probe requires collimated yet not entirely overlapping beams. Collimation is critical because the distance from the probe to tissue might vary, which would strongly affect the size and overlap of

non-collimated beams, and would thus disturb the spatial gating of the diffuse and backscattering components. Potential complication here is the fact that the fiber core diameter itself serves as an extended source. If the fiber core periphery is considered as a point source, and if the refractive collimating lens acts as an aperture stop for the system, the chief ray of this point source forms a non-negligible angle with respect to the optical axis. Indeed, as one can see in Fig. 2, which is a schematic diagram of a fiber with a refractive collimating lens, the associated spot on the tissue, D, is considerably larger than the fiber core diameter, d, due also to the finite numerical aperture (NA) of the fiber. Hence, the illumination/collection spot diameter D on the tissue is governed by two factors—the fiber NA and core diameter. To achieve successful spatial gating, the illumination and collection fibers must each be no closer together than D. A further complexity of this design is the requirement that all optical and structural elements be packaged within the 540 μ m internal diameter of the FNA needle.

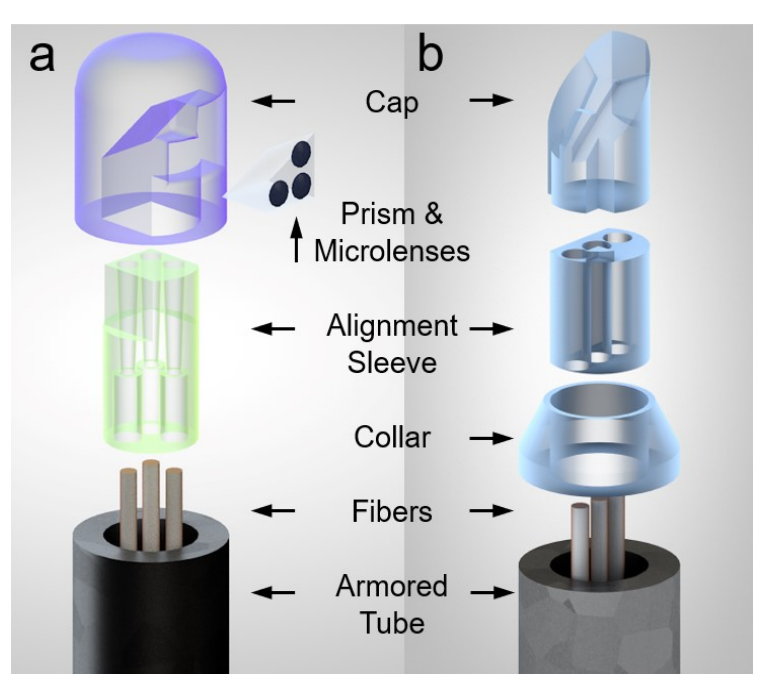


Fig. 3. Design of the distal tip of the refractive and reflective spatial gating non-contact probes. SolidWorks rendering of the distal tip of the (a) refractive and (b) reflective probes.

To ensure proper spatial gating operation of the probe, it should feature three collimated beams, one for the illumination of the cyst surface and two for the collection of scattered light at two different source–detector separations. That can be achieved by using either a refractive or reflective optical arrangement (see Fig. 3), discussed below.

2.2 Refractive non-contact side-looking probe

We first designed a prototype side-looking refractive probe compatible with an 18-gauge aspiration needle. The design of the probe is shown schematically in Fig. 3(a). Several elements here require two-photon polymerization nanofabrication: three microlenses, an alignment sleeve, and a protective rounded cap. An alignment sleeve is used to position three optical fibers—one source and two collection—in a triangular layout, providing two distinct source—detector fiber separations. Light emerging from or going to the fibers reflects off the prism hypotenuse and is collimated by three microlenses. The prism is protected by a rounded cap, and fits within an armored tube, which is inserted into the fine aspiration needle during the ESU-FNA procedure. The probe employs a 700 μ m microprism and three 5 μ m core diameter with 170 μ m cladding diameter single-mode fibers. Using OpticStudio optical design software, the optimal radius of curvature of the plano-convex microlenses was found to be 253 μ m if fabricated with the high optical quality photoresist having a refractive index of 1.514 at a wavelength of λ = 588 nm [15]. The lenses have a central thickness of 15 μ m.

Such probes are designed to be operated with the collimating lens at a relatively fixed distance L from the tissue. If the fiber is a distance I from the collimating lens, then the tissue spot diameter due to the fiber core diameter I is given by simply by I that is, the closer the fiber is to the collimating lens, the more considerable is the effect of core diameter I. Now considering the effect of fiber NA, if the fiber were a point source, then the tissue

spot diameter would be given by the relationship 2l tan(sin⁻¹(NA/n)), where n is the refractive index of the medium between the fiber and collimating lens; i.e., smaller l gives a smaller tissue spot size. Last, considering both effects, the total tissue spot diameter D is given, to first approximation, by

$$D = \frac{2l^2NA + nLd}{nl} \ . \tag{1}$$

We should note, however, that the above probe design is not optimal. The probe uses a fiber with NA = 0.14, placed into contact with the microprism of refractive index n=1.46. Because the prism side length is 700 µm, the fiber-lens distance I can have a minimum value of 700 µm. The probe is designed to be used at a lens-tissue distance of L=10 mm, typical for the studied pre-malignant and malignant cysts, resulting in the contributions to tissue spot diameter D shown in Fig. 4(a). In the design of such probes, space is at a minimum. The smallest tissue spot diameter D, and hence the smallest allowable fiber separation, occurs at one particular fiber-lens separation, found analytically from the preceding equation to occur at $I=(nLd/(2NA))^{1/2}$. Figure 4(a) shows, for the above probe, a minimum value of D at $I\approx 500$ µm; however, the layout of that probe does not allow a lens-fiber separation of less than 700 µm, because the microprism acts as a physical stop. In addition, the smallest allowable fiber separation is approximately 200 µm, implying that the microprism of 700 µm side length is oversized.

Based on the design considerations for the 19-gauge aspiration needle compatible probe described above, we also designed an ultracompact, 22-gauge needle compatible probe, more appropriate for the routine EUS-FNA procedures in pancreatic cysts. For this probe, it was decided to choose a fiber with a slightly larger core diameter of $d=10~\mu\text{m}$, to improve efficiency of scattered light coupling and relax the tolerancing of both microlens fabrication

and microlens–fiber alignment. With the goal of fitting within the small 22-gauge needle, we chose a microprism of 300 μ m side length. Shown as the solid trace in Fig. 4(b) is the tissue spot diameter for a commercially available fiber with $d=10~\mu$ m and NA = 0.1. It can be seen that the smallest fiber separation is $\approx 250~\mu$ m, which makes good use of the microprism side area. This separation is achievable with these fibers, which have a cladding diameter of 125 μ m. The minimum of D occurs at a fiber–lens separation of $I\approx 870~\mu$ m, implying that the fibers cannot be placed against the prism face, but must be kept a distance away maintained by a spacer. For this reason, the plots in Fig. 4(b) use an approximate refractive index of n=1.5 for the material between fiber and lens.

The preceding analysis is very useful in instructing the optical design procedure; however, further miniaturization requires numerical simulation using ray tracing software such as OpticStudio. This is because in reality, the fiber angular illumination profile is not uniform out to the marginal zone of the light cone NA—the intensity of the fiber core emission falls off with radial distance from the fiber center, and the NA of the fiber may also depend upon this radial coordinate. Moreover, the preceding analysis does not consider diffraction. However, the diameter of the Airy disk, given by $2.44\lambda L/a$, where λ is the wavelength of light and a is the diameter of the microlens, is $\approx 80~\mu m$ at $\lambda = 500~nm$, which is negligible compared to D above. Therefore, the further-miniaturized side-looking probe was designed in OpticStudio ray tracing software using non-sequential mode. The latter two illumination effects mentioned above, associated with fiber core radial coordinate, were accounted for by modeling the source fiber using the OpticStudio-supplied source dynamic linked library "fiber1.dll".

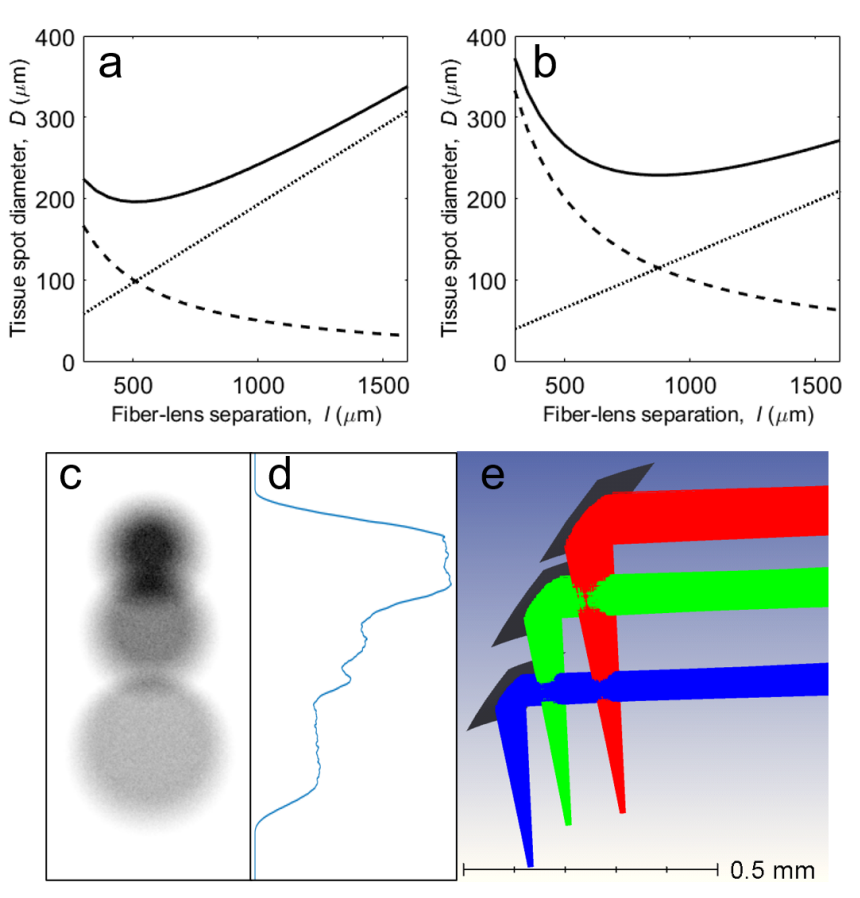


Fig. 4. Tissue spot diameter and spatial distribution of illumination and collection spots on tissue. Tissue spot diameter is based on Eq. (1) and plotted vs fiber–lens separation due to fiber core diameter d (dashed line) and NA (dotted line), combining to give a total diameter D (solid line) at a fiber–tissue distance of L=10 mm. (a) d=5 μ m, NA = 0.14 and n=1.46. (b) d=10 μ m, NA = 0.1 and n=1.5. (c) OpticStudio simulation of the reflective probe spatial beams distribution on tissue, showing one illumination and two collection spots on tissue with L=10 mm. (d) Profile of illumination and collection spots through the central illumination axis. (e) Rendering of the off-axis parabolic mirrors used in a and b.

2.3 Reflective non-contact side-looking probe

The above refractive designs use high quality prisms and require manufacturing of only small parts, reducing time and possible scattering due to any imperfections in the resin polymerization process. A drawback of those designs is a dependence on the refractive index difference at the microlens curved surface. That is, the probe performance depends strongly on the probe immersion medium. Lack of knowledge of the immersion medium

during the EUS-FNA optical biopsy procedure makes the probe performance uncertain—this uncertainty was removed by designing a reflective probe.

The reflective design uses off-axis parabolic mirrors to replace both the microprism cube and laser-written microlenses (see Fig. 3(b)). The use of parabolic mirrors makes the collimation performance of this probe independent of the immersion medium—the light will be collimated if the probe is used in, for example, air or water. An armored tube is terminated by a rounded cap, into which three optical fibers are inserted—as before, the probe again features three collimated beams, one for illumination and two for scattered light collection. The cap consists of three off-axis parabolic mirrors that bend the illumination light perpendicular to the optical axis and collimate the beam. The rear-side of the mirrors is left open, allowing for metallic sputtering of the parabolic profiles, to generate a highly reflective surface. The three optical fibers (NA = 0.1) are placed in contact with the bottom circular, flat face of the cap. The parabolic mirrors collimate the light, which passes through a flattened section of the curved cylindrical surface, a distance of \approx 10 mm from the cyst internal wall. The total light path through the cap is on the order of 1 mm.

The mirror shapes were mathematically derived and were incorporated into the cap designed in SolidWorks. The completed CAD design was exported to a stereolithography file format and imported into OpticStudio ray-tracing software to perform a final check of the model performance after file conversion. Shown in Fig. 4(c) is the illumination spot size at a distance of L = 10 mm, with a profile through the central illumination axis shown in Fig. 4(d). Figure 4(e) is a schematic of the OpticStudio non-sequential modeling procedure. Due to the extended fiber core size, perfect collimation is not possible, and spot separation improves with decreasing fiber–tissue distance L; however, the spots are still separated at the relatively large distance of 10 mm.

3. RESULTS

As outlined above, several elements of the first prototype of the ultracompact refractive non-contact side-looking probe require nanofabrication, and that includes one of the world's smallest microlenses ever manufactured, at just 15 µm thick. To manufacture these microlenses, we employed a nanofabrication system based on two-photon polymerization technology (Nanoscribe Photonic Professional GT2, Nanoscribe GmbH, Germany). The lens CAD design, generated in SolidWorks, was exported to a stereolithography file format, with settings optimized to achieve fine polygon tessellation. Settings for laser-writing were then defined in the DeScribe software (see Fig. 5(a)). The microlenses were manufactured layer-by-layer, referred to as slicing, with layers being 100 nm apart. The lateral resolution, which is referred to as hatching, was also set to 100 nm. Because each of the three microlenses was less than 300 µm in diameter, the writing procedure could be broken into three distinct parts, resulting in no stitching artifacts usually associated with larger procedures.

The uncured refractive index of the chosen IP-L 780 photoresist dictated the choice of the writing substrate, as the uncured photoresist refractive index must be sufficiently different from that of the substrate for the two-photon polymerization system to find the writing interface. Because the uncured refractive index is significantly lower than that of the cured resin, borosilicate D263, with a relatively high refractive index of 1.523 (λ = 588 nm), was chosen for a substrate with thickness of 170 ± 10 µm. Other photoresist and substrate combinations with smaller refractive index difference are possible if the interface can be manually located, and custom GWL programming scripts can be written for those fabrication tasks—such a methodology was used during the laser-writing of lenses directly on a microprism surface, as outlined below.

Before laser-writing, a single droplet of IP-L 780 photoresist was placed on the substrate with the resin bottle spatula. Although preparation and identification of the proper parameters for manufacturing the microlenses using this two-photon polymerization of photoresist took several months and multiple attempts, the actual laser-writing job with identified optimal parameters required less than 2 hours. Upon finishing the two-photon polymerization laser-writing, the microlenses and substrate were taken to a wet bench, where they were left in a 30 mL beaker of PGMEA developer solution (Baker BTS-220) for 20 minutes, and then rinsed in a 30 mL beaker of isopropanol for 5 minutes. After a light blow dry with nitrogen, the microlenses were ready for use. Figure 5(b–e) shows the process and results of the laser-writing task.

We should note here that such small lenses could be susceptible to misalignment during assembly. In an improvement of the design mentioned above, for the actual probe the three microlenses were directly laser-written onto the flat face of the prism, eliminating a crucial source of error in the previous probe assembly. A laser-written prism holder secured the 300 µm prism in place with the reflective hypotenuse at a 45-degree angle to the horizontal. A custom GWL programming script was then used to locate the prism-resin interface and the lenses were laser-written directly on one of the flat faces. The sag profile of a sample lens fabricated with this method was experimentally verified using a transmission holographic system and is shown as the circles in Fig. 5(c), which coincides almost exactly with the OpticStudio model profile (line).

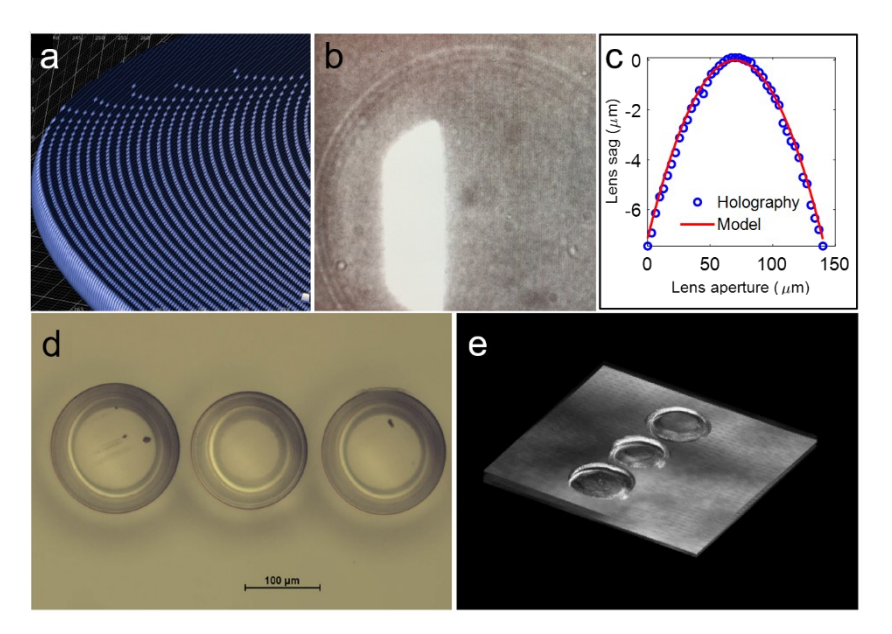


Fig. 5. Two-photon polymerization fabrication of the system of microlenses. (a) Preview of one of the microlenses with the slicer assistant embedded in the DeScribe software, with individual 100 nm voxels clearly seen. (b) Laserwriting of one of the microlenses—the vertical bright line is the reflection of the femtosecond laser beam that polymerizes the photoresist. (c) Height reconstruction of one of the microlenses using transmission holography (circles), coinciding with the OpticStudio model profile (line). (d) Brightfield microscopy image of the microlens system. (e) Image of the microlens system 3D reconstructed from a *z*-stack of confocal reflectance microscopy images.

To construct the side looking optical probe we assembled the microprism with microlenses printed on it, the cap and the alignment sleeves. To assemble these components, we employed two stereoscopes positioned perpendicular to each other, a micromanipulator, a pair of tweezers, and a UV light source for UV-curing of epoxy. Every assembly step was performed under observation with the stereoscopes. When assembling the refractive probe, a very small amount of epoxy glue was placed on the inclined plane of the 300 µm right-angled prism, which was inserted into the protective cap, as shown in Fig. 3, and cured with UV light for one hour. To prepare for fiber installation, we mounted the alignment sleeve on a V-groove clamp using Teflon tweezers and dipped the tip of each single mode fiber into the epoxy. Each fiber was then inserted fully into the holes in the alignment sleeve and

illuminated with UV light for one hour to cure. After that, the alignment sleeve with epoxy glue on top was inserted into the protective cap and attached to the right-angled prism. Finally, all parts were once again illuminated with the UV light source to ensure that they were securely connected. The procedure for assembling the reflective probe was similar.

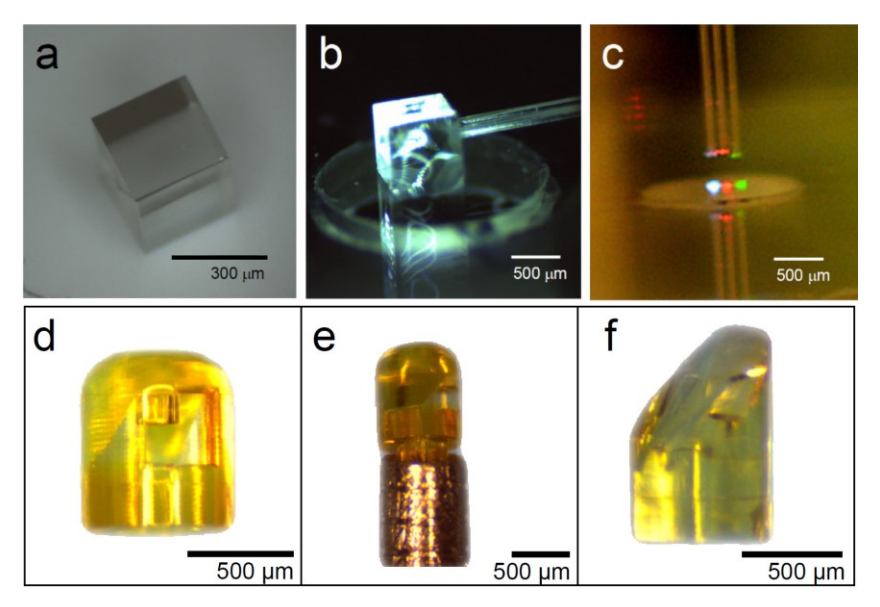


Fig. 6. Two-photon polymerization nanofabricated ultracompact refractive and reflective LSS probes. (a) Microprism cube for refractive probe. (b) Fibers deliver light to the microprism cube. (c) Three 150 μ m diameter beams collimated by microlenses and emitted by the prototype ultracompact side-looking non-contact refractive probe. (d) Nanofabricated and (e) assembled refractive and (f) reflective probes, imaged with yellow illumination for better contrast.

In the refractive probe, three identical microlenses were employed, with one of the microlenses providing a collimated illumination beam and two others serving to collect reflected photons at two source-detector distances. To test the probe, we delivered light through all fibers and observed three collimated light beams of similar diameter (Fig. 6(c)). This distribution of light is very similar to that observed in the existing forward-looking contact probe [6]. When the spacer (alignment sleeve) was employed to improve the quality of the collimation, the divergence of the beams was rather low at 0.27°, and diameters of the beams were observed to be approximately 150 µm at various distances along the beam

paths. Therefore, the probe should maintain good spatial gating capabilities even in large cysts up to 3 cm in diameter.

In the reflective probe, the optical power is controlled entirely by the curvature of the mirror. However, unlike in the refractive probe, the distances between each of the three linearly arranged fibers and the mirrors are different. Hence, the beams here have different diameters of approximately 70 μ m, 90 μ m and 110 μ m, respectively. Due to the compact size of this probe and the finite size of the fiber cores, the divergence of these beams is slightly larger than in the refractive probe. This probe should work well for slightly smaller cysts up to 2 cm in diameter. Manufacturing a micron-scale reflective system of the required high quality is challenging with conventional methods, as the off-axis parabolic mirrors for this probe are among the smallest ever constructed. A uniquely challenging aspect of the reflective design is that the parts contain minute detail and must be of optical quality, but are also relatively large. To avoid diffractive artifacts, the quality must be on the order of the wavelength of light, whereas the entire cap is on the order of hundreds of microns or more. The micro-components were laser-written with IP-S resin, chosen as it performs well for relatively large parts with such high resolution. Figure 6(f) shows a brightfield microscope image of the successfully manufactured reflective probe.

4. CONCLUSION

A significant challenge in the design and manufacture of ultracompact spatial gating light scattering spectroscopic probes is the incorporation of both folding and focusing optics into such a small cylindrical profile for the EUS-FNA procedures in pancreatic cysts. This has been made possible by the two-photon polymerization process, which also drastically improves and simplifies assembly by removing alignment steps. Through consideration of

the fiber NA and diameter, spatial separation of the tissue illumination and collection spots can be achieved even at spatial scales such as those required by the small, 540 µm internal diameter, 22-gauge FNA needle. The refractive probes described here make convenient use of commercially available microprisms to reduce manufacturing time and ensure excellent optical clarity of the probe. Compared to the forward-looking contact probe we recently designed, manufactured and successfully tested in human subjects to differentiate pancreatic cancer cysts and cysts having malignant potential from benign cysts [6], these side-looking probes will allow surveillance of significantly larger areas of the pancreatic cyst wall in a fraction of the time currently spent for the EUS-FNA procedure, enabling more rapid and more accurate "optical biopsy" acquisition.

The arrival of commercially available two-photon fabrication systems does not just allow the manufacture of miniature optics alone—the ability to laser-write complex objects with optical clarity at macro-scales, and to laser-write directly onto existing optics, allows the fabrication of high-quality, well aligned optical research devices at a level not previously attainable by the typical non-commercial research group. The two ultracompact probes described here—one refractive and one reflective—can fit within a 22-gauge EUS-FNA needle, making the optical biopsy minimally invasive. This will further our ultimate goal of improving patient diagnosis and/or drastically improving quality of life, or even extending lifetime for those suffering from a type of cancer having one of the worst prognoses.

Acknowledgments

This work was supported by US National Science Foundation grants EFRI-1830878, CBET-1605116, and CBET-1948722 and US National Institutes of Health grants R01 CA228029, R01 EB003472, R01 CA205431, R01 EB025173, and R01 CA218382.

Competing financial interests

The authors declare no competing financial interests.

References

- A. Semaan and A. Maitra. "Rebooting pancreatic cancer knowledge and treatment options," Nat. Rev. Gastroenterol. Hepatol. 15, 76–78 (2018). DOI: 10.1038/nrgastro.2017.182
- E. A. Collisson, A. Sadanandam, P. Olson, W. J. Gibb, M. Truitt, S. Gu, J. Cooc, J. Weinkle, G. E. Kim, L. Jakkula, H. S. Feiler, A. H. Ko, A. B. Olshen, K. L. Danenberg, M. A. Tempero, P. T. Spellman, D. Hanahan, and J. W. Gray, "Subtypes of pancreatic ductal adenocarcinoma and their differing responses to therapy," Nat. Med. 17, 500–503 (2011). DOI: 10.1038/nm.2344
- 3. W. R. Brugge, G. Y. Lauwers, D. Sahani, C. Fernandez-del Castillo, and A. L. Warshaw, "Cystic neoplasms of the pancreas," N. Engl. J. Med. **351**, 1218–1226 (2004). DOI: 10.1056/NEJMra031623
- W. R. Brugge, K. Lewandrowski, E. Lee-Lewandrowski, B. A. Centeno, T. Szydlo, S. Regan, C. F. del Castillo, and A. L. Warshaw, "Diagnosis of pancreatic cystic neoplasms: a report of the cooperative pancreatic cyst study," Gastroenterology 126, 1330–1336 (2004). DOI: 10.1053/j.gastro.2004.02.013
- 5. S. Cizginer, B. Turner, A. R. Bilge, C. Karaca, M. B. Pitman, and W. R. Brugge, "Cyst fluid carcinoembryonic antigen is an accurate diagnostic marker of pancreatic mucinous cysts," Pancreas **40**, 1024–1028 (2011). DOI: 10.1097/MPA.0b013e31821bd62f
- L. Zhang, D. K. Pleskow, V. Turzhitsky, E. U. Yee, T. M. Berzin, M. Sawhney, S. Shinagare, E. Vitkin, Y. Zakharov, U. Khan, F. Wang, J. D. Goldsmith, S. Goldberg, R. Chuttani, I. Itzkan, L. Qiu, and L. T. Perelman, "Light scattering spectroscopy identifies the malignant potential of pancreatic cysts during endoscopy," Nat. Biomed. Eng. 1, 0040 (2017). DOI: 10.1038/s41551-017-0040
- L. T. Perelman, V. Backman, M. Wallace, G. Zonios, R. Manoharan, A. Nusrat, S. Shields, M. Seiler, C. Lima, T. Hamano, I. Itzkan, J. Van Dam, J. M. Crawford, and M. S. Feld, "Observation of periodic fine structure in reflectance from biological tissue: A new technique for measuring nuclear size distribution," Phys. Rev. Lett. 80, 627–630 (1998). DOI: 10.1103/PhysRevLett.80.627
- 8. L. Qiu, D. K. Pleskow, R. Chuttani, E. Vitkin, J. Leyden, N. Ozden, S. Itani, L. Guo, A. Sacks, J. D. Goldsmith, M. D. Modell, E. B. Hanlon, I. Itzkan, and L. T. Perelman, "Multispectral scanning during endoscopy guides biopsy of dysplasia in Barrett's esophagus," Nat. Med. **16**, 603–606 (2010). DOI: 10.1038/nm.2138
- 9. K. Sokolov, R. Drezek, K. Gossage, and R. Richards-Kortum, "Reflectance spectroscopy with polarized light: is it sensitive to cellular and nuclear morphology," Opt. Express **5**, 302–317 (1999). DOI: 10.1364/OE.5.000302
- 10. C.-C. Yu, C. Lau, J. W. Tunnell, M. Hunter, M. Kalashnikov, C. Fang-Yen, S. F. Fulghum, K. Badizadegan, R. R. Dasari, and M. S. Feld, "Assessing epithelial cell nuclear

- morphology by using azimuthal light scattering spectroscopy," Opt. Lett. **31**, 3119–3121 (2006). DOI: 10.1364/OL.31.003119
- N. G. Terry, Y. Zhu, M. T. Rinehart, W. J. Brown, S. C. Gebhart, S. Bright, E. Carretta, C. G. Ziefle, M. Panjehpour, J. Galanko, R. D. Madanick, E. S. Dellon, D. Trembath, A. Bennett, J. R. Goldblum, B. F. Overholt, J. T. Woosley, N. J. Shaheen, and A. Wax, "Detection of dysplasia in Barrett's esophagus with *in vivo* depth-resolved nuclear morphology measurements," Gastroenterology 140, 42–50 (2011). DOI: 10.1053/j.gastro.2010.09.008
- 12. L. Qiu, V. Turzhitsky, R. Chuttani, D. K. Pleskow, J. D. Goldsmith, L. Guo, E. Vitkin, I. Itzkan, E. B. Hanlon, and L. T. Perelman, "Spectral imaging with scattered light: From early cancer detection to cell biology," IEEE J. Sel. Top. Quantum Electron. **18**, 1073–1083 (2012). DOI: 10.1109/JSTQE.2011.2161575
- A. Wax and K. J. Chalut, "Nuclear morphology measurements with angle-resolved low coherence interferometry for application to cell biology and early cancer detection," Anal. Cell. Pathol. 34, 597970 (2011). DOI: 10.3233/ACP-2011-0017
- 14. T. Gissibl, S. Thiele, A. Herkommer, and H. Giessen, "Two-photon direct laser-writing of ultracompact multi-lens objectives," Nat. Photonics **10**, 554–560 (2016). DOI: 10.1038/nphoton.2016.121
- 15. T. Gissibl, S. Wagner, J. Sykora, M. Schmid, and H. Giessen, "Refractive index measurements of photo-resists for three-dimensional direct laser-writing," Opt. Mater. Express **7**, 2293–2298 (2017). DOI: 10.1364/OME.7.002293